CHAPTER 20

Mountain Waves

Dale R. Durran

20.1. Introduction

The basic flow pattern across a long ridge of mountains is determined by the mountain width. If the ridge is wide enough that the time required for air to cross it is greater than order $1/f$ (where f is the Coriolis parameter), rotational effects generate a disturbance with large displacements in the horizontal x-y plane. As the width decreases to less than 100 km, the perturbations in the horizontal plane disappear and waves in the vertical x-z plane develop. When the wind blows over such a ridge, air parcels are displaced vertically and, if the atmosphere is stably stratified, they descend and may oscillate about their equilibrium levels. The gravity waves that result, called mountain waves or lee waves, have been observed in mountainous regions all over the world.

The presence of mountain waves is frequently revealed by distinctive orographic clouds that form in the wave crests. Various types of mountain waves produce the different types of wave clouds. An identification of a particular type of wave cloud can be used to make some qualitative deductions about the vertical variation in wind speed and stability over the mountains.

Large-amplitude mountain waves can produce several weather phenomena that significantly affect human activity and therefore require the attention of the weather forecaster. The strong downslope winds observed along the lee slopes of mountain barriers are usually associated with large-amplitude waves. Dangerous regions of clear-air turbulence are also produced by these waves.

20.2. Theory of Linear Waves Forced by Sinusoidal Mountain Ridges

The most fundamental properties of mountain waves can be profitably examined by considering the steady-state, two-dimensional airflow over "small-amplitude" mountains (so that linear theory can be used). The two-dimensional assumption is appropriate if the mountains are assumed to extend indefinitely in the direction parallel to the ridge and be sufficiently narrow that the Rossby number governing the flow is large (so Coriolis forces may be neglected). Consider the equations for an inviscid Boussinesq fluid, the simplest case that contains the essential physics governing the flow, and

(consistent with our small-amplitude assumption) linearize them about a horizontally uniform basic state with a mean wind U, a reference potential temperature θ_0, and a mean potential temperature gradient $d\bar{\theta}/dz$. The result may be written

$$U\frac{\partial u}{\partial x} + w\frac{dU}{dz} + \frac{\partial P}{\partial x} = 0 , \tag{20.1}$$

$$U\frac{\partial w}{\partial x} + \frac{\partial P}{\partial z} = b , \tag{20.2}$$

$$U\frac{\partial b}{\partial x} + N^2 w = 0 , \tag{20.3}$$

$$\frac{\partial u}{\partial x} + \frac{\partial w}{\partial z} = 0 , \tag{20.4}$$

where $b = g\theta/\theta_0$, $P = c_p\theta_0\pi$, and $N^2 = (g/\theta_0)(d\bar{\theta}/dz)$. Here (u, w) represent the perturbation velocity components in the Cartesian (x, z) coordinate system, θ is the perturbation potential temperature, and π the perturbation Exner function, $(p/p_0)^{R/c_p}$. The Brunt-Väisälä frequency is given by N. The remaining constants have their conventional meanings.

Equations (20.1)–(20.4) may be combined to form a single equation for w:

$$\frac{\partial^2 w}{\partial z^2} + \frac{\partial^2 w}{\partial x^2} + \ell^2 w = 0 , \tag{20.5}$$

where

$$\ell^2 = \frac{N^2}{U^2} - \frac{1}{U}\frac{d^2U}{dz^2} \tag{20.6}$$

is the Scorer parameter.

As a further simplification, let the terrain profile be defined as an infinite set of periodic ridges,

$$h(x) = h_0 \cos kx , \tag{20.7}$$

and let N and U be constant with height.

Since the Earth's surface is fixed, the normal component of the velocity must vanish at the lower boundary. Thus,

$$w[x, h(x)] = (U + u)\frac{\partial h}{\partial x} , \tag{20.8}$$

which can be approximated, to the same order of accuracy as the linearized equations, as

$$w(x, 0) = U\frac{\partial h}{\partial x} = -Uh_0 k \sin kx . \tag{20.9}$$

Solutions to (20.5) can be obtained in the form

$$w(x,z) = \hat{w}_1(z)\cos kx + \hat{w}_2(z)\sin kx\ . \tag{20.10}$$

Substituting (20.10) into (20.5) yields an equation that determines the vertical structure of the perturbation velocity field. Both $\hat{w}_1$ and $\hat{w}_2$ satisfy

$$\frac{\partial^2 \hat{w}_i}{\partial z^2} + (\ell^2 - k^2)\hat{w}_i = 0 \qquad i = 1,2\ . \tag{20.11}$$

Since N and U are assumed to be constant with height, $\ell^2 - k^2 = m^2$ is a constant and the solution of (20.11) may be written

$$\hat{w}_i(z) = \begin{cases} A_i e^{\mu z} + B_i e^{-\mu z} & k > \ell \\ A_i' \cos mz + B_i' \sin mz & k < \ell\ , \end{cases} \tag{20.12}$$

where $\mu^2 = -m^2$. Note that the vertical structure of the wave depends on the relative magnitudes of the Scorer parameter and the horizontal wavenumber. When $k > \ell$ the wave amplitude decreases (or increases) exponentially with height; when $k < \ell$ the vertical velocity above a fixed point on the ground oscillates between regions of upward and downward motion as z increases.

The coefficients A_i, B_i, A_i', and B_i' in (20.12) are determined by boundary conditions imposed at $z = 0$ and in the limit as z approaches infinity. When $k > \ell$, the first term in the general solution corresponds to a wave whose amplitude grows exponentially without bound as z increases. This behavior is not physically reasonable since the mountain is the energy source for the disturbance. Thus, the boundary condition at infinity requires that $A_i = 0$. Then $B_1 = 0$, $B_2 = -Uh_0k$, in order to satisfy the "tangential flow" condition (20.9).

In the case $k < \ell$, trigonometric identities can be used to write the general solution as

$$\begin{aligned} w(x,z) =& C_1 \sin(kx + mz) + C_2 \sin(kx - mz) \\ &+ C_3 \cos(kx + mz) + C_4 \cos(kx - mz)\ , \end{aligned} \tag{20.13}$$

where both $m > 0$, $k > 0$. The lower boundary condition requires $C_1 + C_2 = -Uh_0k$, and $C_3 + C_4 = 0$. These coefficients are uniquely specified by applying a boundary condition in the limit as z approaches infinity. The nature of this upper boundary condition is not as obvious as it was in the case $k > \ell$, a circumstance that has led to some confusion in the past. The terms with coefficients C_1 and C_3 correspond to waves in which lines of constant phase ($kx + mz$ = constant) tilt upstream. It can be shown that these waves transport energy upward and momentum downward. The opposite is true for the remaining two terms. Since the mountain acts as the energy source for the wave disturbance, the correct choice of coefficients is $C_1 = -Uh_0k$, $C_2 = C_3 = C_4 = 0$, which requires that all energy transport by the waves be directed upward as z approaches infinity.

The same choice of the upstream-tilting wave can be obtained by a variety of other arguments (see Smith, 1979). It should be noted, in particular, that the upstream-tilting wave is invariably obtained as the steady-state numerical solution to initial-value problems involving vertically propagating mountain waves. Unfortunately, some authors continue to suggest that the choice of the upper boundary condition is somehow still an open question. Atkinson (1981) follows Scorer's incorrect development and does not adequately alert the reader that the result for propagating waves, Atkinson's Eq. (34), is wrong.

Perhaps it is easier to understand why the upstream-tilting wave is the correct solution by considering the perturbation pressure field. In this simple situation, the mean wind is constant with height, and the horizontal momentum and continuity equations can be combined to yield

$$\frac{\partial P}{\partial x} = U\frac{\partial w}{\partial z} . \tag{20.14}$$

In the case $k < \ell$, the solutions for the perturbation pressure fields in the upstream- and downstream-tilting waves are

$$P = \begin{cases} -U^2 h_0 m \sin(kx + mz) & \text{upstream tilting} \\ U^2 h_0 m \sin(kx - mz) & \text{downstream tilting} . \end{cases} \tag{20.15}$$

Note that at $z = 0$, the extrema in the perturbation pressure field are shifted 90°relative to the location of the troughs and ridges in topography. The wave that tilts upstream with height $[-\sin(kx+mz)]$ produces high pressure upwind of the ridge crest and low pressure downwind. The wave that tilts downstream produces the opposite pressure pattern. The asymmetry in the pressure distribution across the ridge gives rise to a net pressure force on the topography. The upstream-tilting wave exerts a force on the mountain in the direction of the mean flow, and therefore an equal and opposite force is exerted by the terrain, which acts to decelerate the mean flow. In the case of downstream-tilting waves, the resulting pressure forces are directed upstream and simultaneously accelerate the mean flow in the direction it is already going. This last situation is clearly contrary to physical intuition, suggesting that the correct solution is the upstream-tilting wave.

In summary, the perturbation vertical velocity field in the waves forced by the sinusoidal terrain profile (20.7) can be written

$$w(x,z) = \begin{cases} -Uh_0 k e^{-\mu z}\sin kx & k > \ell \\ -Uh_0 k \sin(kx + mz) & k < \ell . \end{cases} \tag{20.16}$$

The two types of wave structures are illustrated in Fig. 20.1. The waves in the case $k > \ell$ (Fig. 20.1a) decay exponentially with height (evanescent waves), whereas in the $k < \ell$ case (Fig. 20.1b), the waves propagate vertically, without loss of amplitude.

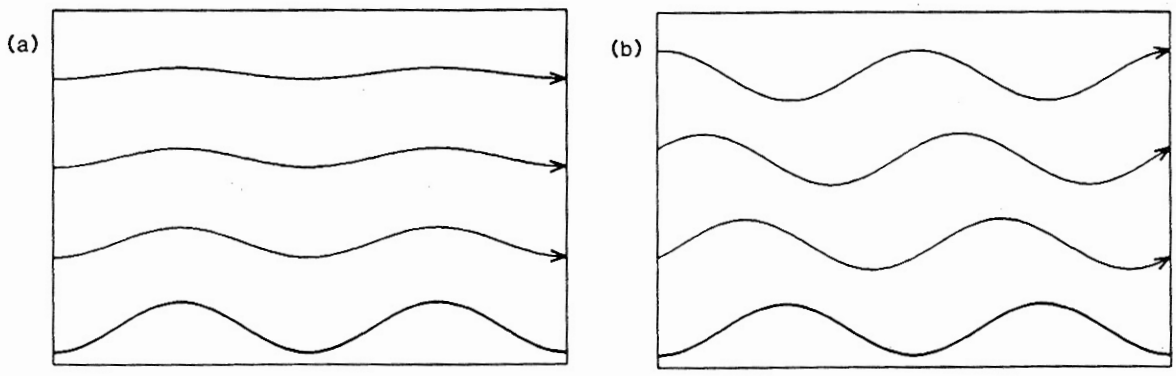

Figure 20.1. Streamlines in the steady airflow over an infinite series of sinusoidal ridges when (a) the wavenumber of the topography exceeds the Scorer parameter (narrow ridges) or (b) the wavenumber of the topography is less than the Scorer parameter (wide ridges).

The speed of the air flowing through these waves can also be determined from Fig. 20.1. It follows from the change in spacing between streamlines, which in this case are actually contours of a stream function, that in the case of the vertically propagating wave there will be weak winds over the windward slope and strong winds in the lee. This amplification of the lee-side wind is believed to be associated with the development of strong downslope winds like the Colorado chinook. In the case of the evanescent wave, the distribution of wind speed is symmetric about the mountain peak, the strongest winds being directly above the crest.

The physical reason for the difference between the two types of waves may be described qualitatively as follows. The requirement $k < \ell$ is equivalent, in the absence of curvature in the mean wind profile, to $Uk < N$, which states that the intrinsic frequency of the forcing by the terrain must be less than the Brunt-Väisälä frequency. The Brunt-Väisälä frequency is the highest frequency at which buoyancy forces can support periodic motion in a stably stratified fluid; parcels of air oscillating at the Brunt-Väisälä frequency move vertically, straight up and down. Lower frequency oscillations are obtained when the parcel paths are tilted at some angle off the vertical. It can be shown that if ϕ is the angle between the slanted parcel trajectories and the vertical, the frequency of the oscillation will be $N \cos \phi$ (Gill, 1982, p. 132). The troughs and crests in vertically propagating gravity waves tilt in order to match the natural frequency of the atmospheric oscillations to the intrinsic frequency forced by the airflow over the terrain. As a result, the slope of the wave crests (which is identical to the slope of a parcel trajectory) satisfies

$$Uk = N \cos \phi \, . \tag{20.17}$$

However, if the intrinsic frequency of the forcing exceeds N, no real angle ϕ will satisfy (20.17), and no buoyancy-driven oscillation can be established. In this case, buoyancy forces act to dampen the oscillation, like a spring forced at a nonresonant frequency. The wave are damped more rapidly as the difference between Uk and N increases.

20.3. Theory of Linear Waves in More Realistic Situations

The mountain wave solutions (20.16) apply only to an air mass with constant stability, flowing at a uniform mean speed, across an endless series of sinusoidal ridges. If more realistic terrain profiles and atmospheric structures are considered, other solutions to (20.5) can be obtained which bear a strong resemblance to observed mountain waves. The following is a description of how the wave response is influenced by isolated ridges and vertical variation in the Scorer parameter, the mathematical derivations are often omitted; they may be found in Smith (1979) and Queney *et al.* (1960).

20.3.1. Influence of Shape of Terrain

Suppose the mountain contour consists of a single ridge so that the terrain elevation eventually drops to some reference level at all distances sufficiently far upstream and downstream. Just as Fourier series can be used to represent a wide variety of periodic functions as an infinite sum of sines and cosines, the isolated mountain can, under rather general conditions, be constructed from periodic functions by the use of Fourier transforms. The Fourier transform (F) of a real function ϕ and its inverse (F^{-1}) may be defined:

$$\begin{aligned} \hat{\phi}(k) &= F[\phi(x)] - \frac{1}{\pi}\int_{-\infty}^{\infty} \phi(x) e^{-ikx} dx; \\ \phi(x) &= F^{-1}[\hat{\phi}(k)] = \mathrm{Re}\int_{0}^{\infty} \hat{\phi}(k) e^{ikx} dk \ . \end{aligned} \tag{20.18}$$

The Fourier transform is particularly useful in this application because it has the property that $F(\partial^n \phi/\partial x^n) = (ik)^n \hat{\phi}$.

If the fundamental equation for linear gravity waves (20.5) is Fourier transformed in the horizontal, the result is (20.11), where $\hat{w}(k,z) = F[w(x,z)]$. Thus, the behavior of each component $\hat{w}(k_0,z)$ of the transformed vertical velocity field is identical to that obtained by forcing the atmosphere with sinusoidal topography having the wavenumber k_0. Thus, the results obtained in Sec. 20.2 are also applicable to the case of isolated topography. The only complication arises from the requirement that after $\hat{w}(k,z)$ is determined, the actual vertical velocity field must be recovered by application of the inverse transform.

Consider again the case in which N and U (and hence ℓ) are constant with height. The function $\hat{w}(k,z)$ is the complex analog of (20.12), which, after the free slip and radiation boundary conditions are evaluated, is

$$\hat{w}(k,z) = ikU\hat{h}(k,z)\ \exp[i(\ell^2 - k^2)^{1/2} z] \qquad k > 0 \ . \tag{20.19}$$

Here $\hat{h}$ is the Fourier transform of the terrain profile; it determines the relative weight accorded to each wavenumber in the final solution $w(x,z)$. If the mountain is very narrow, the dominant weighting will be at wavenumbers greater than ℓ so the solution will consist primarily of evanescent waves. On the other hand, if the mountain is sufficiently wide, the dominant weighting

is at wavenumbers less than ℓ and the solution consists primarily of vertically propagating waves.

Figure 20.2 above shows how the waves generated by a bell-shaped ridge,

$$h(x) = \frac{h_0 a^2}{a^2 + x^2} \ , \tag{20.20}$$

vary with the difference between a^{-1} and ℓ (N and U are again constant with height). This mountain has a maximum height of h_0 at $x = 0$, and falls to $\frac{1}{2}h_0$ at $x = \pm a$; thus a^{-1} represents a scale characteristic of the wavenumbers forced by the mountain. For very narrow mountains, where $a^{-1} >> \ell$ (Fig. 20.2a), the wave pattern is symmetric with respect to the ridge crest, and the perturbations decay with height, just like the evanescent waves in Sec. 20.2. For a wide mountain, where $a^{-1} << \ell$ (Fig. 20.2c), the waves propagate vertically, and lines of constant phase tilt upstream. Assuming the condition that $a^{-1} << \ell$ is equivalent to taking the hydrostatic limit, in which case $k << \ell$ and (20.19) reduces to

$$\hat{w}(k,z) = ik\, U\hat{h}(k,z)\, e^{i\ell z} \qquad k > 0 \ , \tag{20.21}$$

eliminating the dependence of vertical wavelength on horizontal wavenumber. As a result, the mountain profile is reproduced at every level that is an integral multiple of $2\pi/\ell$. (This result is independent of the shape of the mountain.)

In the third case, $a^{-1} = \ell$ (Fig. 20.2b), the solution is dominated by vertically propagating nonhydrostatic waves (i.e., $k < \ell$ without $k << \ell$) and the situation is more complicated. The phase lines still tilt upstream, and energy is transported upward. However, unlike hydrostatic waves, in which the transport occurs directly over the mountain (because the horizontal group velocity of a stationary hydrostatic wave is zero), nonhydrostatic waves transport energy both upward and downstream (because the horizontal

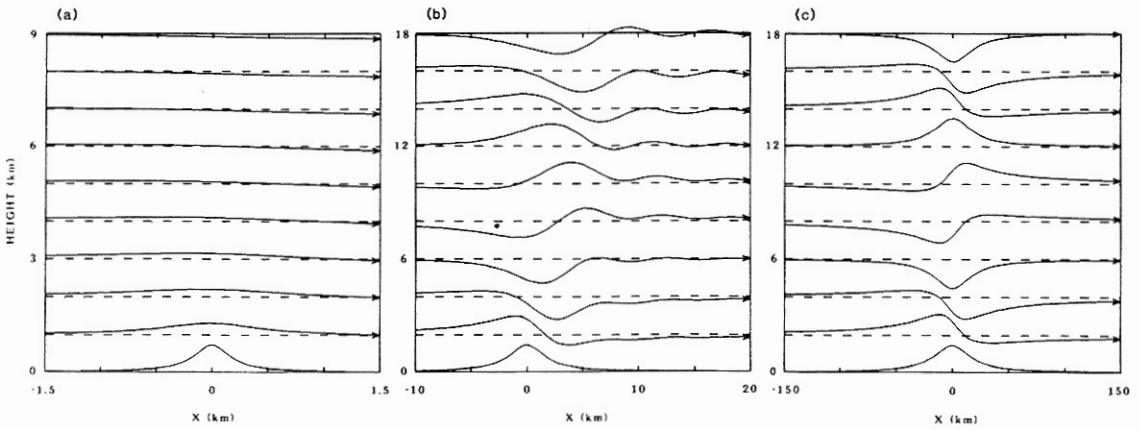

Figure 20.2. Streamlines in the steady airflow over an isolated bell-shaped ridge. (a) $a^{-1} >> \ell$, narrow ridge; (b) $a^{-1} = \ell$, width of the ridge comparable with the Scorer parameter; (c) $a^{-1} << \ell$, wide ridge, but not so wide that rotational effects become significant.

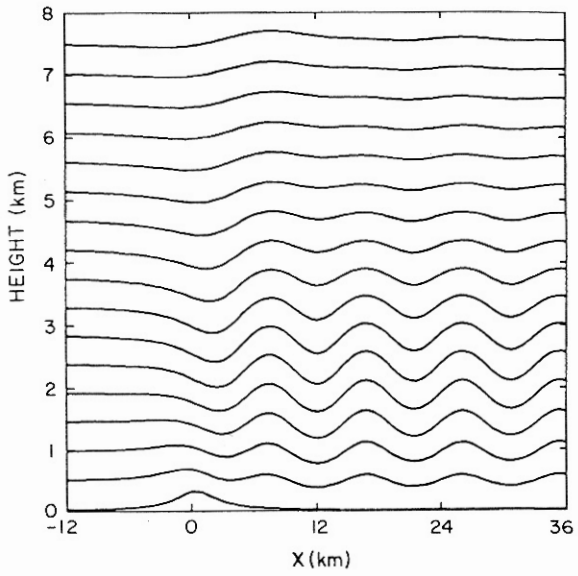

Figure 20.3. Streamlines in the steady airflow over an isolated bell-shaped ridge when the vertical variation of the Scorer parameter has the two-layer structure shown in Fig. 20.4.

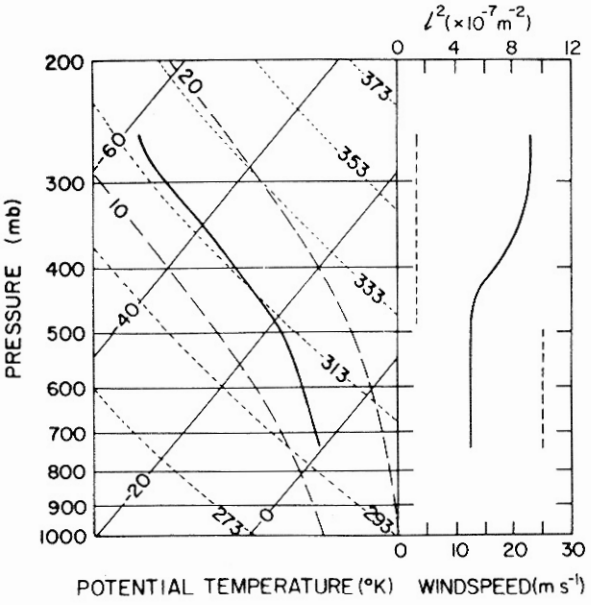

Figure 20.4. A vertical distribution of temperature and wind speed (solid lines), which implies a discontinuous two-layer structure for the Scorer parameter (dashed line on right panel).

group velocity of a stationary nonhydrostatic wave is directed downstream). As a result, the waves in Fig. 20.2b appear in a wedge-shaped region downstream of the ridge.

It is important to appreciate that if a mountain is sufficiently wide to produce essentially hydrostatic waves (but not so wide that Coriolis forces become significant), there will be only one wave crest in the air flowing over the mountain. Additional crests do not appear downstream from the mountain unless nonhydrostatic effects are significant. Even in the case shown in Fig. 20.2b, the wave amplitude decays rapidly downstream from the mountain.

20.3.2. Influence of Atmospheric Structure

Trapped lee waves are a different type of mountain wave. The airflow in a system of trapped waves (also known as resonant lee waves) is shown in Fig. 20.3. Note that most of the wave activity is confined to the lower troposphere on the lee side of the mountain. As demonstrated by Scorer (1949), this type of long wave train occurs only when ℓ^2 decreases with height. Reference to (20.6) reveals that a decrease in ℓ^2 will result from an increase in wind speed, a decrease in stability, or an increase in the curvature of the wind speed profile. Scorer examined the behavior of linear waves in a two-layer atmosphere in which ℓ^2 was constant in each layer. An example of this kind of two-layer structure is shown in Fig. 20.4, which describes the upstream conditions for the solution shown in Fig. 20.3. Note that a discontinuity in ℓ^2 can occur without discontinuities in θ and U. Scorer

showed that the wavenumber of the trapped waves must satisfy the following resonance condition:

$$(\ell_L^2 - k^2)^{1/2} \cot[(\ell_L^2 - k^2)^{1/2} H] = -(k^2 - \ell_U^2)^{1/2} , \tag{20.22}$$

where ℓ_U and ℓ_L are the Scorer parameters in the upper and lower layers, and H is the depth of the lower layer. A necessary condition for the existence of a solution to (20.22) is

$$\ell_L^2 - \ell_U^2 > \frac{\pi^2}{4H^2} , \tag{20.23}$$

which states that the difference in wave propagation characteristics in the two layers must exceed a certain threshold before the waves can be "trapped." If (20.23) is satisfied by a sufficient margin, there may be multiple solutions to (20.22), in which case the mode with the longest horizontal wavelength will usually dominate.

The wavenumber of the resonant wave solution to (20.22) must satisfy the inequality

$$\ell_L > k > \ell_U , \tag{20.24}$$

which implies that the wave propagates vertically in the lower layer, and decays exponentially in the upper layer. One might expect the waves to tilt upstream with height throughout the region in which they are vertically propagating; however, as shown in Fig. 20.3, trapped waves have no tilt. This is because, when the upward-propagating waves (which are originally triggered by the mountain) reach the upper layer, they cannot continue to propagate upward; they are reflected as downward-propagating waves. The downward-propagating waves subsequently are reflected as upward-propagating waves when they strike the ground. As this process continues, an infinite number of reflections take place. There is no loss of amplitude when the waves are reflected because there are no energy exchanges with the upper layer or the flat ground downstream of the mountain. As a result, the disturbances that appear downstream are the superposition of equal-amplitude upward- and downward-propagating waves, and thus have no tilt. To illustrate this mathematically, the trapped waves in Fig. 20.3 have the functional form

$$w(x,z) = \beta \sin \alpha z \cos kx , \tag{20.25}$$

in the lower layer. Here β and α are constants (see Queney *et al.* [1960] for the details). By using trigonometric identities, (20.25) can be written as the sum of two equal amplitude waves that tilt upstream and downstream, respectively:

$$w(x,z) = \frac{\beta}{2} \sin(\alpha z + kx) + \frac{\beta}{2} \sin(\alpha z - kx) . \tag{20.26}$$

Referring again to Fig. 20.3, note that, in addition to the trapped waves, a weak vertically propagating wave also appears over the mountain. This

develops because the mountain produces some forcing at wavenumbers less than ℓ_U, thereby generating waves that can propagate through the upper layer. The mountain shown in Fig. 20.3 is specified by (20.20) with $a = 2.5$ km, $h_0 = 300$ m. If the mountain width is increased, the amplitude of the vertically propagating waves would increase and the amplitude of the trapped waves would decrease.

This example illustrates the important conclusion that the behavior of linear mountain waves depends entirely on the shape of the terrain profile and the mean atmospheric structure. The range of possible wave motions (i.e., which wavelengths will be vertically propagating, which will be evanescent, and which, if any, will be resonant and trapped) is determined by the atmospheric structure, particularly the mean horizontal wind speed and static stability. The shape of the terrain determines the strength of the forcing applied to each wavelength. In most atmospheric situations associated with mountain waves, vertically averaged values of N and U typically lie in the ranges 0.008 to 0.02 s^{-1} and 10 to 40 m s^{-1}, implying that most wavelengths less than 3 km ($k > N_{max}/U_{min}$) will be evanescent, and most wavelengths greater than 30 km ($k < N_{min}/U_{max}$) will propagate vertically. Trapped waves generally occur at intermediate wavelengths between 5 and 25 km.

20.4. Interpretation of Clouds in Satellite Photos

20.4.1. Types of Clouds

Wave-induced orographic clouds are often evident in satellite photographs. However, when interpreting these photographs, operational meteorologists tend to assume that all cloud-producing mountain waves propagate horizontally (Fig. 20.3). In fact, vertically propagating waves (Fig. 20.2c) commonly generate clouds as well, and the two types of clouds can usually be distinguished. Once the type of wave has been indentified, certain general conclusions can be drawn about the atmospheric conditions in the vicinity of the waves.

Clouds From Trapped Waves

The clouds in Fig. 20.5 show an extensive region of lee wave activity covering most of Nevada and portions of Oregon, Idaho, and Utah on 2 May 1984 at 1715 GMT. These are trapped waves of the type shown in Fig. 20.3, and can be recognized as such by these characteristics:

- There are multiple wave crests downstream from the initial disturbance.
- The wavelength, which varies between 10 km in northwestern Nevada and 23 km in southeastern Nevada, lies in the range at which waves are likely to be trapped.

The first waves appear to be generated by the Sierra Nevada and the Cascades, although the continued excitation of trapped waves at distances far downstream is probably produced by the mountains in the basin and range region of Nevada.

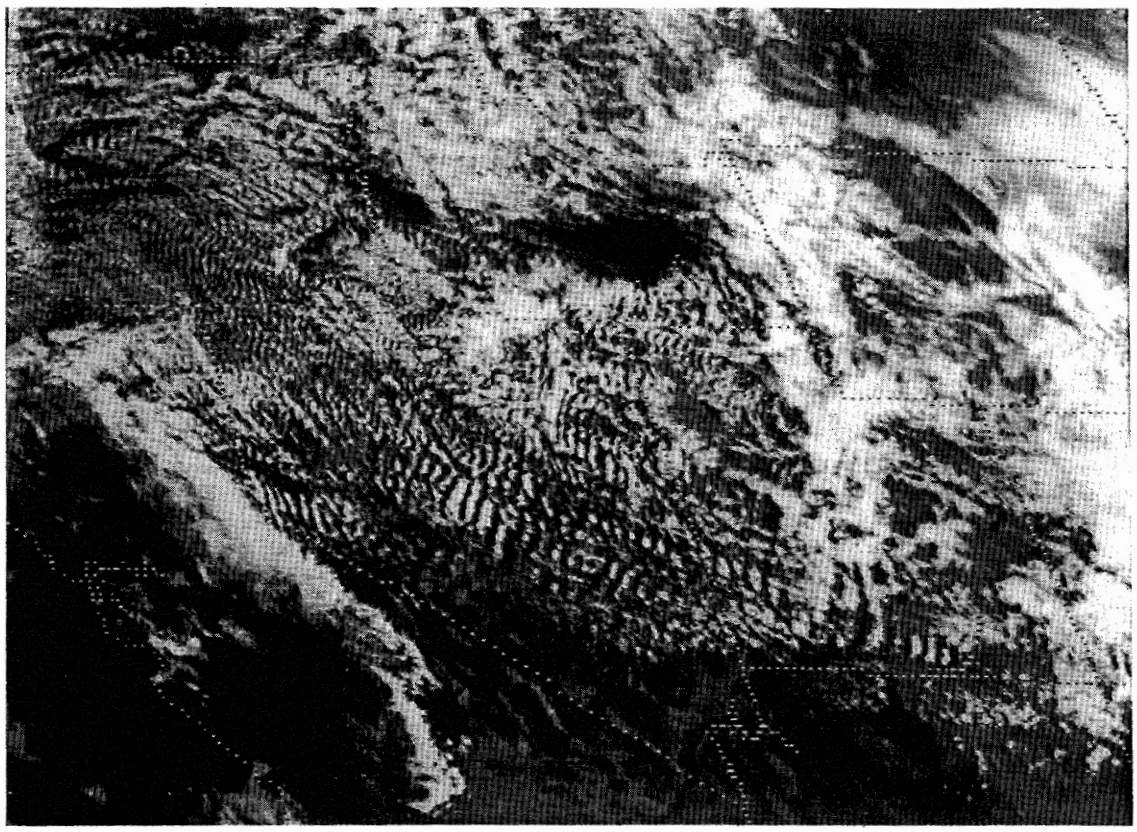

Figure 20.5. Visible satellite imagery for 1715 GMT, 2 May 1984.

Given that the waves revealed in Fig. 20.5 are trapped waves, one can draw general conclusions about the state of the atmosphere in their vicinity. In order for mountain waves of any type to exist, a sufficiently strong wind must be directed across the mountain at the ridge-top level. The minimum wind speed required for waves will vary with the size and shape of the mountain, but seems to lie in the range from 7 to 15 m s^{-1} (Queney *et al.* 1960). Since the waves are trapped, ℓ^2 values in the upper troposphere should be significantly smaller than those in the lower troposphere. This requirement is usually satisfied by a large increase in the wind with height, and the presence of one or more stable layers in the lower troposphere. Fig. 20.6 shows the 700 and 200 mb analyses for this case. Note that the winds are oriented almost perpendicular to the northern Sierras and to the Nevada ranges at both 700 and 200 mb, and there is a dramatic increase in wind speed with height. The thermodynamic properties of this air mass are illustrated in Fig. 20.7 by the Winnemucca sounding taken at 0000 GMT on 3 May. A pronounced stable layer is evident in the lower troposphere; the moist layer that probably contained the wave clouds is also apparent.

Clouds From Vertically Propagating Waves

A different type of situation is shown in Fig. 20.8, in which clouds reveal the presence of mountain waves along the eastern edge of the Front Range of

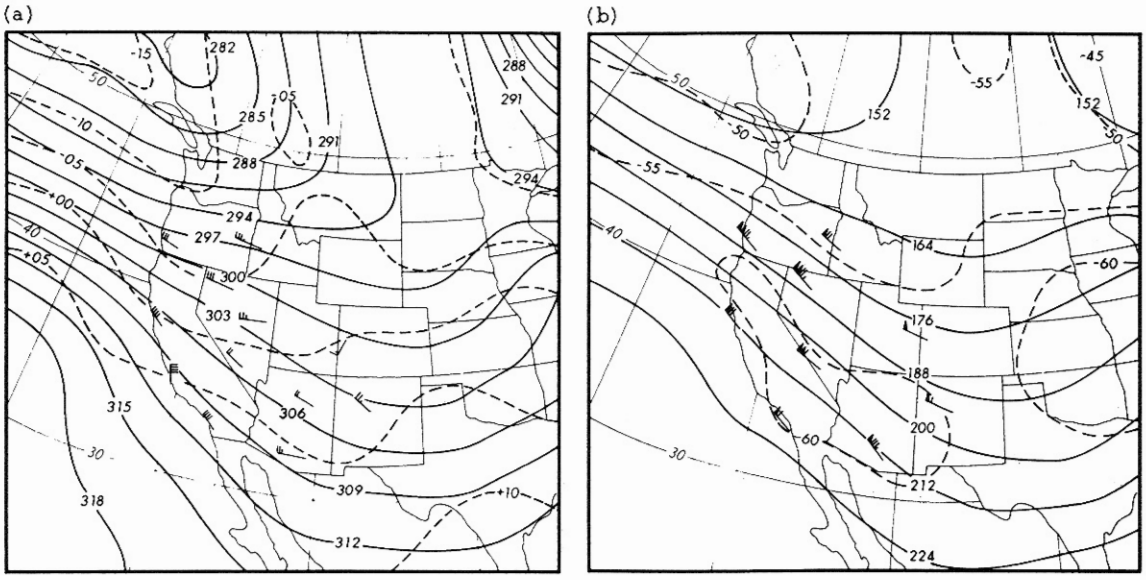

Figure 20.6. Analysis for 1200 GMT, 2 May 1984. (a) 700 mb; (b) 200 mb.

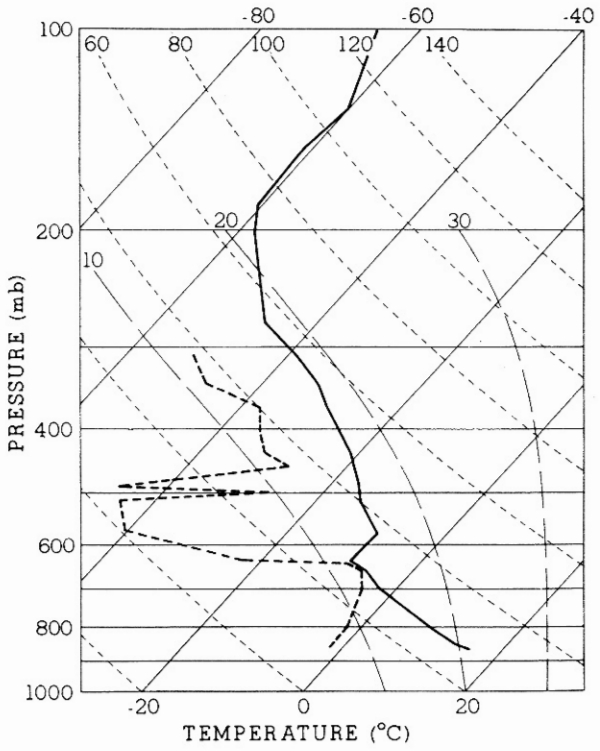

Figure 20.7. Winnemucca sounding for 0000 GMT, 3 May 1984. The 1200 GMT sounding for 2 May is similar, but shows two distinct inversions in the layer between 610 and 460 mb.

Colorado's Rocky Mountains at 1815 GMT on 7 November 1983. One can conclude that the waves are vertically propagating for the following reasons:

- Only one wave crest is visible.
- The horizontal wavelength, though hard to determine, exceeds the width of the wave cloud, which is roughly 100 km. This is far too long a wavelength to be trapped.

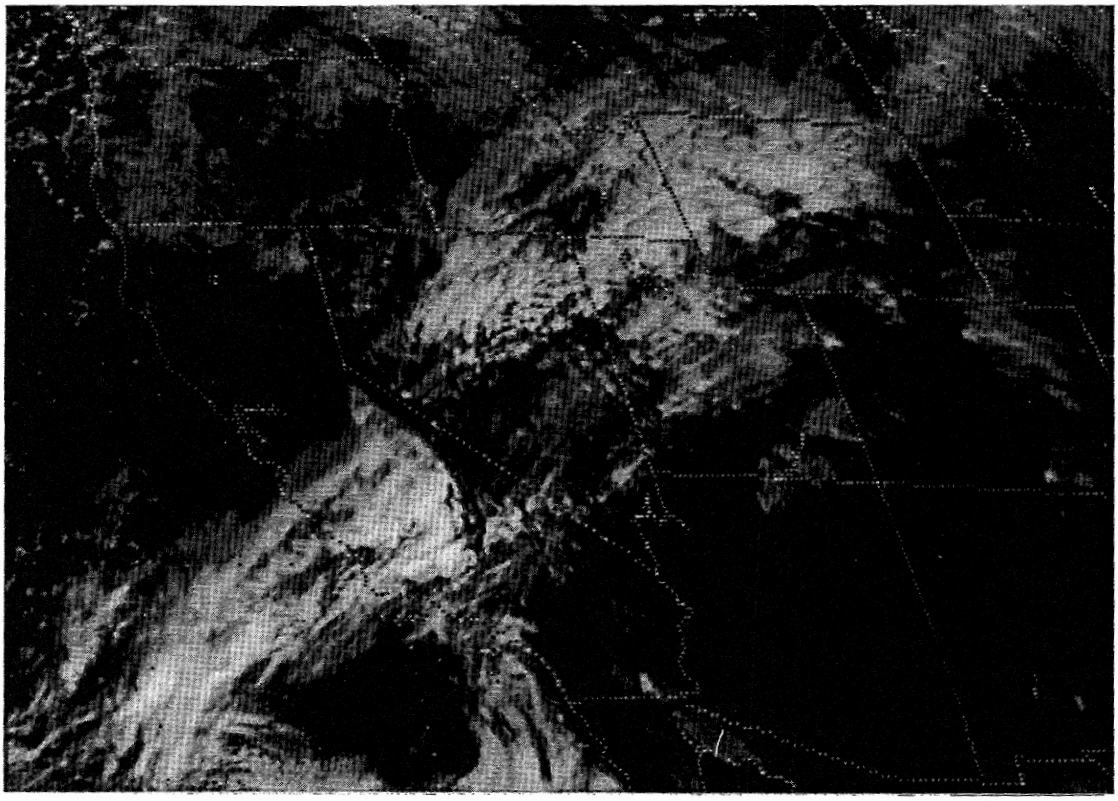

Figure 20.8. Visible satellite imagery for 1815 GMT, 7 November 1983.

Given that the waves are vertically propagating, one should again expect a significant flow across the mountains, but in this case, little can be definitely concluded about the vertical distribution of ℓ^2. As shown in Figs. 20.9 and 20.10, the increase in wind speed with height is less pronounced and the low-level stable layers are weaker than in the previous example. This seems to suggest that the difference between the waves in Figs. 20.5 and 20.8 can be accounted for by differences in the atmospheric conditions (i.e., insufficient decrease in ℓ^2 to trap the waves). However, the most significant difference is probably due to the topography. The Front Range is a wide mountain range so it tends to force long waves, which can propagate vertically even when ℓ^2 is very small. Reliable conclusions about the vertical distribution of wind speed and stability can generally be obtained only when trapped waves are present.

20.4.2. Distribution of Clouds

Returning to Fig. 20.8, note that although the winds over the Sierra Nevada and the Rockies are quite similar, the cloud patterns are just opposite. The clouds are largely restricted to the upwind side of the Sierras, whereas they appear on the downstream side of the Rockies.

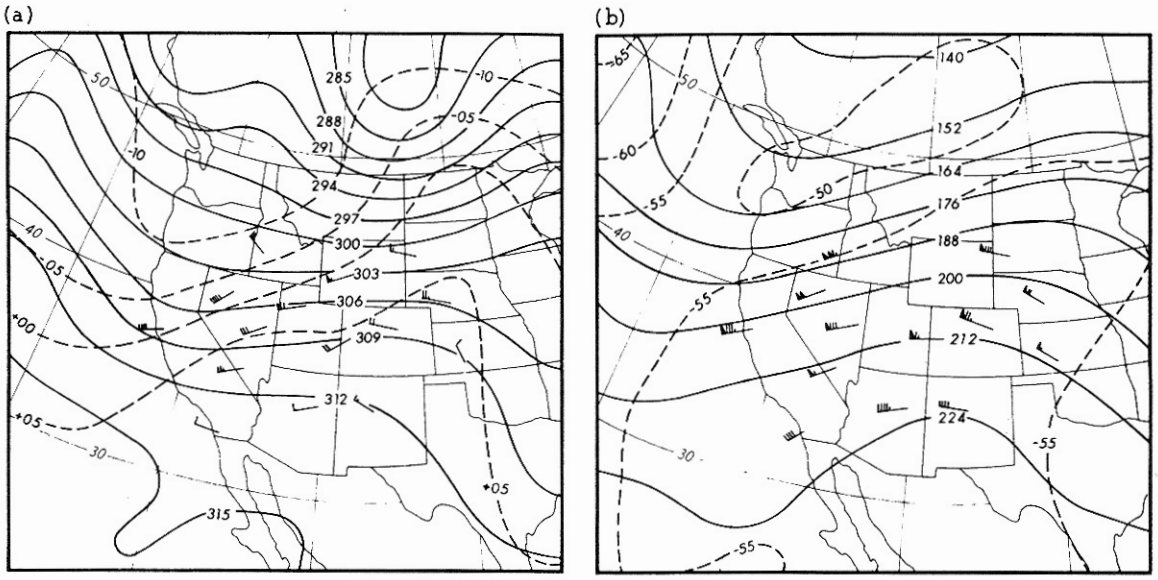

Figure 20.9. Analysis for 1200 GMT, 7 November 1983. (a) 700 mb; (b) 200 mb. The poor agreement between the wind and height fields at 700 mb can probably be attributed to orographic effects.

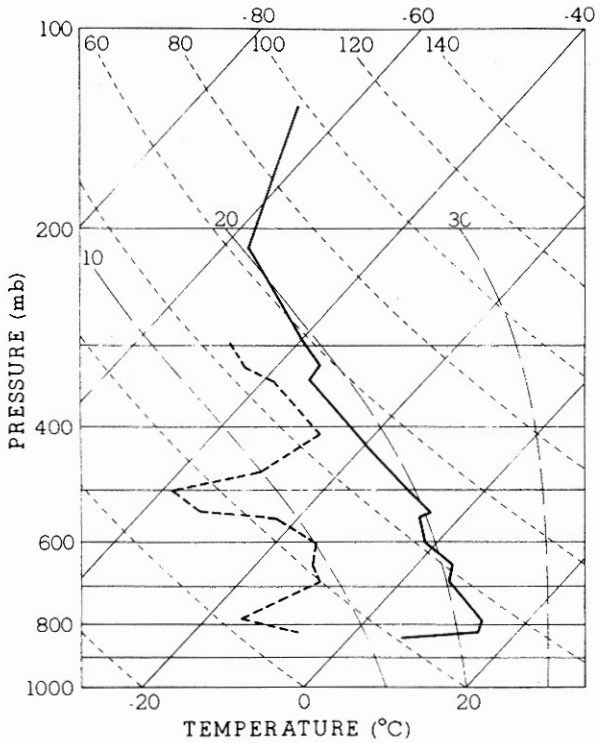

Figure 20.10. Denver sounding taken at 1200 GMT, 7 November 1983.

Middle- and Low-Level Clouds

The difference betweeen the middle- and low-level cloud distributions can be easily accounted for by differences in humidity. The moist maritime air mass flowing inland from the Pacific must be lifted 3 to 4 km to traverse

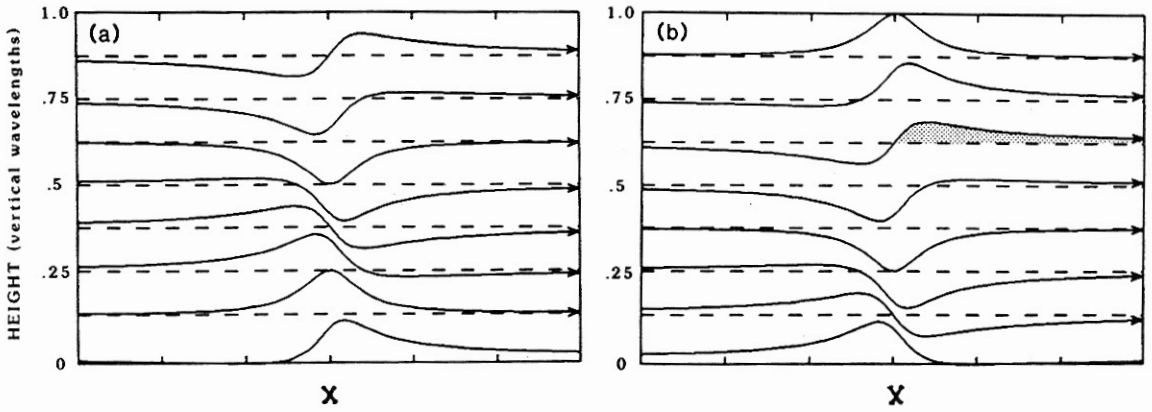

Figure 20.11. Streamlines in the steady airflow over an isolated asymmetric ridge with (a) a steep windward slope; (b) a steep leeward slope. Probable location of wave-induced cirrus is shaded.

the Sierras. In fact, most of the low-level flow is blocked and never passes directly over the main ridge, but there is still sufficient lifting to produce extensive regions of middle- and low-level clouds on the windward side of the mountain. At 1800 GMT (the approximate time of the satellite picture) surface stations upstream of the mountain in the Central Valley report multiple layers of stratiform and cumuliform clouds. On the other hand, no clouds appear upstream of the Colorado Front Range because the air approaching the crest, having already traversed several mountain ranges, is drier, and because less lifting is required to clear the crest of the Front Range. (Less lifting is required to traverse the Rockies because the air upstream starts at the elevation of the high intermountain plateau, not at sea level as in the case of the Sierra Nevada.)

The distribution of low- and middle-level cloudiness is similar in the lee of both mountain ranges. The cloud-free area in the lee of the Sierras, sometimes referred to as a foehn gap, is produced by descending air, which experiences net subsidence since the upstream flow is blocked. An additional contribution to the lee-side clearing occurs as moisture is removed by precipitation over the mountains. Bishop, a surface station on the lee side, reports precipitation in sight but distant from the station, presumably from the foehn (or cap) cloud along the ridge crest. Although it is not obvious from the satellite photo, the lee side of the Rockies is almost clear of middle- and low-level clouds. As in the case of the Sierras, subsidence over the lee slopes produces a reduction of relative humidity. Dry air is apparent below 400 mb in the Denver sounding (Fig. 20.10).

High-Level Clouds

The difference in the distribution of high cloud is harder to explain. One can hypothesize that it is due to differences in the terrain profiles or to moisture effects, or to some combination of the two.

The effect of differences in the terrain shape is illustrated in Fig. 20.11, which shows the linear hydrostatic waves that develop in a Boussinesq fluid flowing with uniform wind speed and stability over asymmetric mountains.

In Figs. 20.11a,b the mountain contours correspond to the fifth and first streamlines above the surface in Fig. 20.2c; the only difference in the three cases is the phase of the disturbance at the ground. Fig. 20.11a shows the streamline pattern forced by a mountain with a steep windward slope and a gentle lee slope. This corresponds to the large-scale character of the Sierras, which rise from sea level on the windward side, but descend only to the level of the intermountain plateau in the lee. In contrast, the Colorado Front Range corresponds to the situation shown in Fig. 20.11b, where the elevation upstream exceeds the elevation in the lee. It must be emphasized that this description applies only to the long wavelength characteristics of the mountain; on a smaller scale, the lee slope of the Sierras descending into Owens Valley is actually steeper than the windward slope. The vertical coordinate in Fig. 20.11 is labeled in vertical wavelengths ($L = 2\pi U/N$). For representative values of N and U, the heights of the high clouds in Fig. 20.8 would lie between $0.5L$ and $0.75L$. At these heights there would be a net downward displacement in the lee of the Sierras (Fig. 20.11a) and a net upward displacement in the lee of the Rockies (Fig. 20.11b), which would produce the observed distribution of high clouds.

A second possible explanation involves the influence of moisture on the flow upstream of the Sierras. Suppose that both ranges are represented by symmetric profiles and that the orographic cloud is forming at a physical height which corresponds to a level of $0.75L$ over the Rockies as illustrated in Fig. 20.12b. Durran and Klemp (1983) have demonstrated that a region of deep cloudiness on the upstream side of a mountain can increase the wavelength in vertically propagating waves by 30%, because the local stability is reduced in the regions where the air is saturated. If the deep clouds upstream of the Sierras were to increase the vertical wavelength by 30% relative to the (dry) value over the Rockies, the same physical height at which orographic cloud appears downstream of the Rockies would correspond to just $0.57L$ over the Sierras, which (as shown in Fig. 20.12a) would be an unfavor-

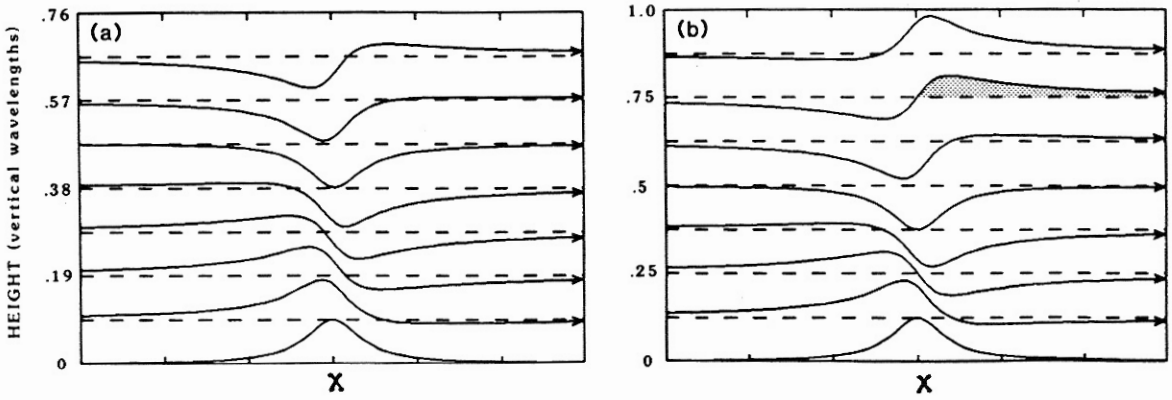

Figure 20.12. Streamlines in the steady airflow over an isolated bell-shaped mountain when the vertical wavelength in (a) exceeds the wavelength in (b) because of a reduction in the stability due to cloudiness over the windward slopes. Probable location of wave-induced cirrus is shaded.

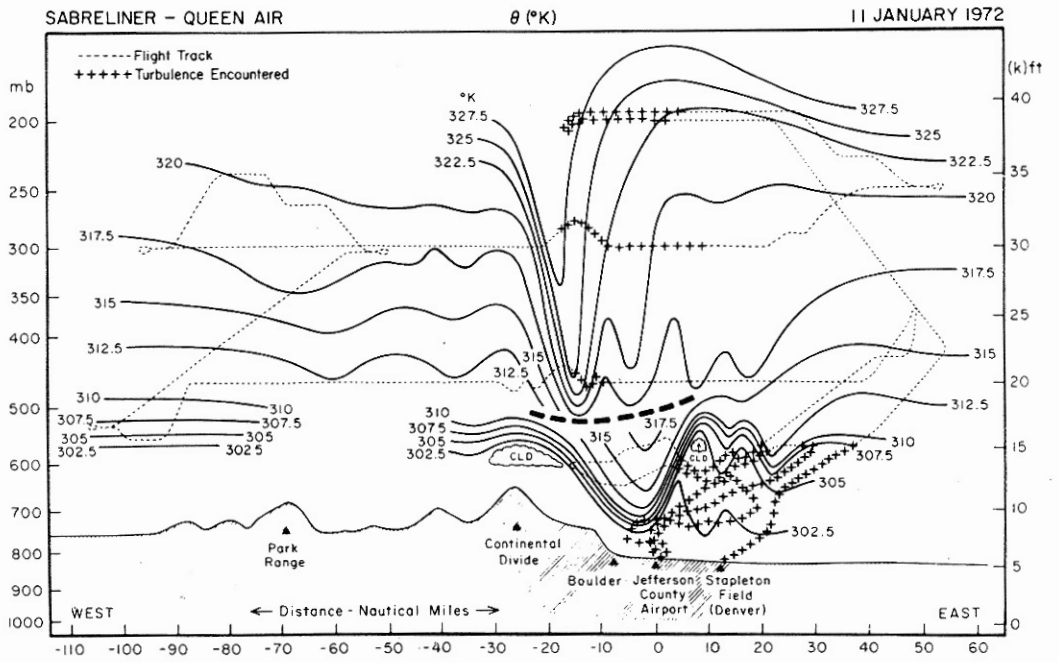

Figure 20.13. Cross section of the potential temperature field observed in a very strong mountain wave over Boulder, Colo., on 11 January 1972. The heavy dashed lines separate observations taken at different times; the dotted lines show the aircraft flight tracks; the crosses indicate regions of turbulence. (From Lilly and Zipser, 1972.)

able region for lee-side cloud development because there is a net downward displacement throughout most of the region.

If the previous two hypotheses are combined, so that the streamlines in Fig. 20.11a are adjusted to reflect an increase in vertical wavelength, the difference between the net vertical displacements in the upper troposphere becomes even more pronounced. A more complete analysis of this case is hampered by the lack of detailed information about the actual cloud levels, and uncertainties about nonlinear effects.

20.5. Development of Large-Amplitude Mountain Waves

The concepts that rely on linear theory (Secs. 20.2–20.3) are implicitly limited to relatively low-amplitude waves. Although they produce impressive cloud formations, these low-amplitude waves have little direct impact on human activities. In contrast, large-amplitude mountain waves can produce damaging downslope winds and dangerous regions of clear-air turbulence. An example of one such large-amplitude wave is shown in Fig. 20.13, which is an analysis of data collected over Boulder, Colo., on 11 January 1972 by Lilly and Zipser (1972). Understanding of the dynamics governing the behavior of large-amplitude mountain waves is, unfortunately, incomplete. Three possible mechanisms have been suggested to explain the development of large-amplitude waves such as the one shown in Fig. 20.13.

20.5.1. Hydraulic Jump

Long (1953) and several subsequent investigators examined hydraulic analogs to the atmosphere consisting of two or more immiscible fluids flowing over a barrier. Long established a set of conditions under which a hydraulic jump will form downstream of the barrier, and suggested that the mechanism that produces the hydraulic jump may be similar to one that produces strong waves and downslope winds in the atmosphere. This approach has the merit of explicitly accounting for the nonlinearities in the system; however, unlike the atmosphere, all the models considered have an upper boundary consisting of either a free surface or a rigid lid. Since no upward energy transport can occur across the upper boundary, vertically propagating atmospheric waves cannot be properly represented in hydraulic models. At any rate, since most of the cases examined have been limited to a fluid with no more than three homogeneous layers (i.e., $N = 0$ in each layer), any comparison of results with waves in the continuously stratified atmosphere must be primarily qualitative.

20.5.2. Reflection of Upward-Propagating Waves

A second mechanism for the generation of large-amplitude waves has been suggested by Klemp and Lilly (1975), who examined the behavior of linear waves in a multilayer atmosphere with constant stability and wind shear in each layer. Unlike Scorer, they limited their investigation to wavelengths that would be long enough to propagate vertically throughout every layer, even those with the smallest values of ℓ (in fact they assumed the waves were hydrostatic). When an upward-propagating wave encounters a region in which the Scorer parameter changes rapidly, part of its energy is reflected back into a downward-propagating wave. The wave amplitude below the reflecting layer is thus determined by the superposition of upward- and downward-propagating waves. Klemp and Lilly found that in the case of a three-layer atmosphere flowing over sinusoidal topography, the optimal superposition occurs when each of the lower layers is one-fourth of a vertical wavelength deep, in which case the downslope wind speed exceeds that which develops in the presence of a single uniform layer by the factor $N_1 N_3 / N_2^2$, where N_1, N_2, and N_3 are the Brunt-Väisälä frequencies in the lower, middle, and upper layers. If the upper layer is assumed to represent the stratosphere, this result suggests that the development of strong waves will be favored when the lower troposphere is relatively stable and the lapse rate in the remainder of the troposphere is nearly dry adiabatic.

The multilayer approach can be extended to more layers, and has the advantage that, as the number of layers is increased, the mean state used in the calculations can be configured to closely match an actual sounding. Klemp and Lilly (1975) used a many-layered model, with reasonable success, to predict downslope winds in Boulder, Colo., from soundings taken upstream. However, since this is a linear model, it must be applied with caution to the case of large-amplitude waves because the perturbation fields in these waves are comparable in magnitude to the mean flow. Recent nu-

merical experiments suggest that, in the case of some large-amplitude waves, the predictions from linear multilayer models can be rather misleading.

20.5.3. Self-Induced Critical Layer

A third mechanism for the generation of large-amplitude waves has been suggested by Clark and Peltier (Clark and Peltier, 1977; Peltier and Clark, 1979). They examined the behavior of large-amplitude mountain waves with a nonlinear nonhydrostatic model, obtaining good agreement between their calculations and the flow observed on 11 January 1972 over Boulder, Colo. (Fig. 20.13). Their numerical approach has the advantage that it explicitly accounts for nonlinear and nonhydrostatic effects, and it allows a detailed representation of the atmospheric flow structure. They observed that a substantial increase in the strength of the wave occurs once the streamlines overturn and the wave "breaks." The wave-breaking region is characterized by strong mixing and a local reversal of the horizontal wind. Clark and Peltier suggest that the energy in the upward-propagating wave is trapped below this self-induced critical layer (the region where the wind reverses direction), thereby producing large-amplitude waves such as the one in Fig. 20.13. A disadvantage to the numerical approach is that the results reflect the highly complex interaction of several factors, and therefore can be rather difficult to interpret. At present, there is still some controversy about the role played by self-induced critical layers on the subsequent amplification of the wave (Lilly and Klemp 1980; Peltier and Clark, 1980).

20.6. Forecasting Mountain Waves

In spite of the advances in our understanding in the last 25 years, it is still not possible to make detailed forecasts of the strength, duration, and precise location of the mountain wave phenomena that occur in the real atmosphere. As a result, little improvement can be made to the forecasting advice offered by Queney *et al.* (1960) and Colson (1954), which was based on a combination of results from linear theory and observational experience. Note, for example, that the work of Peltier and Clark (1979) on the importance of wave overturning provides little guidance to the forecaster trying to assess the potential for wave development from an upstream sounding. One reasonable approach would be to estimate the wave response according to linear theory, and assume that if overturning is predicted it will occur in the actual nonlinear flow as well. In fact, it has not yet been clearly established whether the optimal upstream conditions for linear waves closely coincide with those for large-amplitude waves.

Queney *et al.* (1960) described the conditions in which strong waves are likely to develop:

- The mountain barrier in question has a steep lee slope. Theoretical support for this once largely empirical criterion was obtained by Smith (1977) and Lilly and Klemp (1979), who confirmed that asymmetric mountains with steep leeward and gentle windward slopes are the most effective generators of large-amplitude mountain waves.

- The wind is directed across the mountain (roughly within 30°of perpendicular to the ridge line) throughout a deep layer of the troposphere. The wind speed at the level of the crest should exceed a terrain-dependent value of 7 to 15 m s^{-1}, and should increase with height.
- The upstream temperature profile exhibits an inversion or a layer of strong stability near mountain top height, with weaker stability at higher levels. Colson (1954) also suggested that weak stability below the inversion favors the development of waves in the lee of the Sierra Nevada.

These conditions were originally established in order to predict trapped waves, so that the second and the third imply a decrease in the Scorer parameter with height, between the inversion and the tropopause. The evaluation of an approximation to the Scorer parameter,

$$\ell^* = \frac{N}{U} , \tag{20.27}$$

is also recommended. (The U_{zz}/U term is not always negligible, but is omitted because it is difficult to evaluate from the radiosonde reports available in an operational environment.) Waves will be favored whenever the ℓ^* profile decreases significantly with height.

The importance of vertically propagating waves and the role played by the stratosphere have been recognized only in the last decade. The guidelines for forecasting vertically propagating waves, based again on linear theory and observations, are identical to conditions described by Queney *et al.* (1969) and listed above, except for the role played by wind speed (the wind direction and minimum speed criteria are unchanged). In the case of trapped waves, an increase in the wind speed with height produces a decrease in ℓ^*, enhancing the potential for wave trapping, so that roughly speaking, the stronger the upper level winds, the greater the chance for lee waves. Klemp and Lilly (1975) showed that the amplitude of vertically propagating waves reaches a maximum when the phase shift between the ground and the tropopause is one-half vertical wavelength. This implies that for a given stability profile, the optimal wind speed distribution should satisfy

$$\pi = \int_{z_s}^{z_t} \ell^* ds , \tag{20.28}$$

where z_t is the height of the tropopause and z_s is the height of the topography or the top of a blocked layer of air upstream of the mountain, and $\pi = 3.1416$. If the stability distribution is suitable for intense waves, strong upper tropospheric winds will generally be required to satisfy (20.28), but the presence of very strong winds aloft (as in the case of the jet stream) will not necessarily favor the development of large-amplitude vertically propagating waves.

If strong waves of any type are forecast, clear-air turbulence and downslope winds are likely to develop as well. When the potential for downslope winds is estimated, the synoptic-scale pressure gradient across the mountains

should also be considered. As discussed in Sec. 20.2, mountain waves generate a mesoscale pressure distribution with high pressure upstream of the crest and low pressure in the lee. Strong downslope winds are more likely to develop when the synoptic-scale pressure gradient is in phase with the wave-induced pressure gradient. For example, the strongest Colorado chinooks occur during wave events when there is a large region of high pressure upstream of the mountains to the west, and a rapidly developing lee-side trough or low pressure center in the high plains to the east or northeast.

REFERENCES

Atkinson, B. W., 1981: *Meso-Scale Atmospheric Circulations.* Academic Press, New York, 496 pp.

Clark, T. L., and W. R. Peltier, 1977: On the evolution and stability of finite-amplitude mountain waves. *J. Atmos. Sci.*, **34**, 1715–1730.

Colson, D., 1954: Meteorological problems in forecasting mountain waves. *Bull. Amer. Meteor. Soc.*, **35**, 363–371.

Durran, D. R., and J. B. Klemp, 1983: A compressible model for the simulation of moist mountain waves. *Mon. Wea. Rev.*, **111**, 2341–2361.

Gill, A. E., 1982: *Atmosphere-Ocean Dynamics.* Academic Press, New York, 662 pp.

Klemp, J. B., and D. K. Lilly, 1975: The dynamics of wave-induced downslope winds. *J. Atmos. Sci.*, **32**, 320–339.

Lilly, D. K., and J. B. Klemp, 1979: The effects of terrain shape on non-linear hydrostatic mountain waves. *J. Fluid Mech.*, **95**, 241–261.

Lilly, D. K., and J. B. Klemp, 1980: Comments on "The evolution and stability of finite-amplitude mountain waves. Part II: Surface wave drag and severe downslope windstorms." *J. Atmos. Sci.*, **37**, 2119–2121.

Lilly, D. K., and E. J. Zipser, 1972: The front range windstorm of 11 January 1972—a meteorological narrative. *Weatherwise*, **25**, 56–63.

Long, R. R., 1953: A laboratory model resembling the "Bishop-wave" phenomenon. *Bull. Amer. Meteor. Soc.*, **34**, 205–211.

Peltier, W. R., and T. L. Clark, 1979: The evolution and stability of finite-amplitude mountain waves. Part II: Surface wave drag and severe downslope windstorms. *J. Atmos. Sci.*, **36**, 1498–1529.

Peltier, W. R., and T. L. Clark, 1980: Reply. *J. Atmos. Sci.*, **37**, 2122–2125.

Queney, P., G. Corby, N. Gerbier, H. Koschmieder, and J. Zierep, 1960: The airflow over mountains. WMO Tech. Note 34, 135 pp.

Scorer, R., 1949: Theory of waves in the lee of mountains. *Quart. J. Roy. Meteor. Soc.*, **75**, 41–56.

Smith, R. B., 1977: The steepening of hydrostatic mountain waves. *J. Atmos. Sci.*, **34**, 1634–1654.

Smith, R. B., 1979: The influence of mountains on the atmosphere. In *Advances in Geophysics*, **21**, Academic Press, New York, 87–230.